

Probing the optical chiral response of single nanoparticles with optical tweezers

R. Ali,^{1,*} R. S. Dutra,² F. A. Pinheiro,¹ F. S. S. Rosa,¹ and P. A. Maia Neto¹

¹*Instituto de Física, Universidade Federal do Rio de Janeiro,
Caixa Postal 68528, Rio de Janeiro, RJ, 21941-972, Brasil*

²*LISComp-IFRJ, Instituto Federal de Educação, Ciência e Tecnologia,
Rua Sebastião de Lacerda, Paracambi, RJ, 26600-000, Brasil*

(Dated: June 9, 2020)

We propose an enantioselective scheme to sort homogeneous chiral particles using optical tweezers. For a certain range of material parameters, we show that a highly focused circularly-polarized laser beam traps particles of a specific chirality selected by the handedness of the trapping beam. Furthermore, by applying a transverse Stokes drag force that displaces the trapped particle off-axis, we allow for the rotation of the particle center-of-mass around the trapping beam axis. The rotation angle is highly dependent on the handedness of the trapped particle and is easily measurable with standard video-microscopy techniques, allowing for an alternative mechanism for chiral resolution. Our platform not only allows for enantioselection of particles dispersed in solution but also paves the way to the characterization of the chiral parameter of individual, homogeneous chiral microspheres using optical tweezing.

I. INTRODUCTION

Chiral structures are ubiquitous in nature and play a crucial role in the biological functions of living species. Natural chiral substances have also fundamental technological and industrial importance as they are present in many chemical and pharmaceutical compounds [1]. Natural optical activity is the hallmark optical effect exhibited by chiral media, as discovered in the pioneering work by Arago, and it is typically weak for naturally occurring materials [1]. With advent of metamaterials and plasmonics, new artificial media with much higher chiral optical response have been developed to generate novel optical properties and applications such as negative index media [2, 3], broadband circular polarizers [4], and enantioselective photochemistry [5]. An important class of artificial chiral media is composed of plasmonic nanoparticles, which includes chiral nanocrystals, DNA-assembled plasmonic nanostructures, chiral plasmonic particles assembled on scaffolds, core-shell plasmonic spheres [6–8], and assemblies of nanoparticles in chiral configurations, such as helices [9] or even random arrangements [10]. However, it is quite challenging to probe individual chiral optical response for single chiral plasmonic nanoparticles, as the existing enantioselective methods usually can only measure the average chiral optical response of a large number of (typically) non-identical particles in solution (e.g. circular dichroism). By the same token, no established method exists to determine the chiral parameter κ of individual nanoparticles, which would be of great interest to characterise optical chiral response in chiral nanoplasmonics [11, 12].

To circumvent these limitations, we have recently put forward an alternative chiral resolution method to not only achieve enantioselection of chiral nanoparticles but

also to determine their chiral parameter κ [13]. This method is based on optical tweezing of dielectric spheres coated with chiral shells, where it is possible to select the handedness of the trapped coated particles by choosing the appropriate circular polarization of the trapping laser beam. Our approach compares favorably with previous proposals [14–30] and implementations [31–38] of optical chiral resolution as it allows for the determination of the chiral parameter of each individual trapped nanoparticle via the rotation of the equilibrium position under the effect of a transverse drag force. However, this method has only been applied so far to coated nanoparticles. The case of homogeneous chiral nanoparticles is not only different from a physical point of view, as their light scattering properties are distinct from coated ones, but also is more relevant for a number of chiral systems, such as chiral plasmonic nanocrystals [39]. Here we show that our method can be applied to micrometer sized homogeneous chiral spheres. In addition, we provide a detailed derivation of our theoretical approach, which is based on a generalization of the Mie-Debye theory of optical tweezers [40, 41] to the case of chiral trapped particles.

This paper is organized as follows. In section II, we review the basic formalism of electromagnetic scattering by a chiral sphere using the formalism of Debye potentials. In addition, the optical torque exerted on trapped chiral particles is discussed in detail. In Sec. III, we present our results and discuss how the chirality affects the condition for optical tweezing. Finally, in Sec. IV we summarise our findings and conclusions.

II. METHODOLOGY

A. Electromagnetic fields in chiral media

In a chiral medium, the electromagnetic fields \mathbf{E} and \mathbf{H} are coupled by a chirality parameter κ . The constitutive

*r.ali@if.ufrj.br

relations may be written as [42–44]

$$\begin{aligned}\mathbf{D} &= \epsilon_0 \epsilon \mathbf{E} + i\kappa \sqrt{\epsilon_0 \mu_0} \mathbf{H} \\ \mathbf{B} &= -i\kappa \sqrt{\epsilon_0 \mu_0} \mathbf{E} + \mu \mu_0 \mathbf{H}\end{aligned}\quad (1)$$

where \mathbf{D} and \mathbf{B} are the electric displacement and the magnetic field in the chiral material, respectively. Furthermore, ϵ , μ are the effective relative permittivity and permeability of the medium, and ϵ_0 , μ_0 are the absolute permittivity and permeability of vacuum.

The Maxwell's equations for chiral media in the frequency domain can be compactly written in a matrix form with the help of the constitutive relations (1) as

$$\nabla \cdot \begin{bmatrix} \mathbf{E} \\ \mathbf{H} \end{bmatrix} = 0 \quad , \quad \nabla \times \begin{bmatrix} \mathbf{E} \\ \mathbf{H} \end{bmatrix} = K \begin{bmatrix} \mathbf{E} \\ \mathbf{H} \end{bmatrix}\quad (2)$$

where

$$K = \begin{bmatrix} k_0 \kappa & ik_0 \mu \sqrt{\mu_0 / \epsilon_0} \\ -ik_0 \epsilon \sqrt{\epsilon_0 / \mu_0} & k_0 \kappa \end{bmatrix}.$$

and $k_0 = \omega \sqrt{\mu_0 \epsilon_0} = \omega / c$. In addition, a direct inspection of (1) shows that the transverse character of \mathbf{E} and \mathbf{H} is only ensured if $\mu \epsilon \neq \kappa^2$, so we assume that such condition holds from now onwards [45]. By introducing a linear transformation A , also known as Bohren decomposition, that mixes \mathbf{E} and \mathbf{H} [43, 46]

$$\begin{bmatrix} \mathbf{\Lambda}_+ \\ \mathbf{\Lambda}_- \end{bmatrix} = \frac{1}{2} \begin{bmatrix} \sqrt{\mu_0 / \epsilon_0} & i\sqrt{\mu / \epsilon} \\ i\sqrt{\epsilon / \mu} & \sqrt{\epsilon_0 / \mu_0} \end{bmatrix} \begin{bmatrix} \mathbf{E} \\ \mathbf{H} \end{bmatrix} = A \begin{bmatrix} \mathbf{E} \\ \mathbf{H} \end{bmatrix}, \quad (3)$$

it is simple to show that we get uncoupled Helmholtz equations for each of the vectors $\mathbf{\Lambda}_\sigma$, $\sigma = \pm 1$:

$$\nabla^2 \mathbf{\Lambda}_\sigma + k_\sigma^2 \mathbf{\Lambda}_\sigma = \mathbf{0} \quad (4)$$

where $k_\sigma = k_0(\sqrt{\mu \epsilon} - \sigma \kappa)$. The parameter σ represents the helicity of the propagating waves, as $\mathbf{\Lambda}_+$ and $\mathbf{\Lambda}_-$ are left- and right-hand eigenmodes of incident circularly polarized waves that independently satisfy the Maxwell's equations in the frequency domain. Finally, given the dispersion relation for k_σ , it is convenient to define a chiral refraction index m_σ

$$m_\sigma = \sqrt{\mu \epsilon} - \sigma \kappa \quad (5)$$

that effectively characterizes the propagation of circularly polarized waves of helicity σ .

B. Mie series solution for a chiral sphere

The solution of the Helmholtz equation (4) in spherical coordinates is thoroughly discussed in the literature [46, 47], but the chiral case presents a non-trivial additional element: while propagating eigenmodes correspond to the vector fields $\mathbf{\Lambda}_\sigma$, the boundary conditions involve the fields $\mathbf{E}, \mathbf{D}, \mathbf{B}$ and \mathbf{H} . Fortunately, the linear relation (3) allows a straightforward solution for the

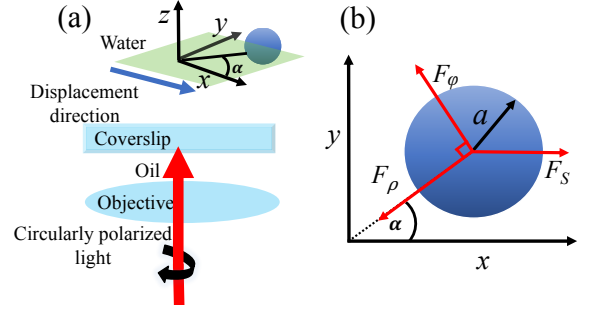


FIG. 1: (a) Schematic representation of enantioselective optical tweezing. A single circularly-polarized Gaussian laser beam is focused at the focal plane of the objective lens in order to optically trap homogeneous chiral microspheres dispersed in aqueous solution. The sample is driven laterally at a constant speed. (b) As the trapped sphere is laterally displaced by the resulting Stokes drag force F_S , its equilibrium position rotates around the optical z axis by an angle α . The cylindrical optical force components F_ρ and F_ϕ are shown.

scattered field by a chiral sphere (given an incident plane wave) [43, 46, 48]:

$$\begin{aligned}\mathbf{E}_s &= E_0 \sum_{\ell} (i)^{\ell} \frac{2\ell + 1}{\ell(\ell + 1)} (ia_{\ell} N_{e1\ell}^3 \\ &\quad - b_{\ell} M_{o1\ell}^3 + c_{\ell} M_{e1\ell}^3 - id_{\ell} N_{o1\ell}^3) \\ \mathbf{H}_s &= \frac{k}{\omega \mu} E_0 \sum_{\ell} (i)^{\ell} \frac{2\ell + 1}{\ell(\ell + 1)} (a_{\ell} M_{e1\ell}^3 \\ &\quad + ib_{\ell} N_{o1\ell}^3 - ic_{\ell} N_{e1\ell}^3 - d_{\ell} M_{o1\ell}^3),\end{aligned}\quad (6)$$

where $M_{e1\ell}^3$, $M_{o1\ell}^3$, $N_{e1\ell}^3$ and $N_{o1\ell}^3$ are the vector spherical harmonics [46]. The scattering amplitudes a_{ℓ} , b_{ℓ} , c_{ℓ} and d_{ℓ} are commonly known as Mie coefficients [43, 44, 46, 48, 49]

$$\begin{aligned}a_{\ell} &= \frac{V_{\ell}(-)A_{\ell}(+) + V_{\ell}(+)A_{\ell}(-)}{W_{\ell}(+)V_{\ell}(-) + V_{\ell}(+)W_{\ell}(-)} \\ b_{\ell} &= \frac{W_{\ell}(+)B_{\ell}(-) + W_{\ell}(-)B_{\ell}(+)}{W_{\ell}(+)V_{\ell}(-) + V_{\ell}(+)W_{\ell}(-)} \\ c_{\ell} &= -d_{\ell} = i \frac{W_{\ell}(-)A_{\ell}(+) - W_{\ell}(+)A_{\ell}(-)}{W_{\ell}(+)V_{\ell}(-) + V_{\ell}(+)W_{\ell}(-)}\end{aligned}\quad (7)$$

with

$$\begin{aligned}W_{\ell}(\sigma) &= m\psi_{\ell}(y_{\sigma})\xi'_{\ell}(x) - \xi_{\ell}(x)\psi'_{\ell}(y_{\sigma}) \\ V_{\ell}(\sigma) &= \psi_{\ell}(y_{\sigma})\xi'_{\ell}(x) - m\xi_{\ell}(x)\psi'_{\ell}(y_{\sigma}) \\ A_{\ell}(\sigma) &= m\psi_{\ell}(y_{\sigma})\psi'_{\ell}(x) - \psi_{\ell}(x)\psi'_{\ell}(y_{\sigma}) \\ B_{\ell}(\sigma) &= \psi_{\ell}(y_{\sigma})\psi'_{\ell}(x) - m\psi_{\ell}(x)\psi'_{\ell}(y_{\sigma})\end{aligned}\quad (8)$$

where $m = m_+ m_- / 2(m_+ + m_-)$. The Riccati-Bessel functions [50] ψ_{ℓ} , ξ_{ℓ} are evaluated either at the size parameter $x = \sqrt{\epsilon_w} k_0 a$ defined with respect to the wavelength in the non-magnetic achiral host medium (relative

electric permittivity ϵ_w) or at $y_\sigma = m_\sigma x / \sqrt{\epsilon_w}$. Finally, for future convenience, we introduce the Debye potentials Π^E and Π^M for electric and magnetic multipoles [47]

$$\begin{aligned}\Pi^E(\mathbf{r}) &= \sum_{\ell}^{\infty} \frac{(\mathbf{r} \cdot \mathbf{E})}{\ell(\ell+1)} \\ \Pi^M(\mathbf{r}) &= \sum_{\ell}^{\infty} \frac{(\mathbf{r} \cdot \mathbf{H})}{\ell(\ell+1)},\end{aligned}\quad (9)$$

which satisfy a (scalar) Helmholtz equation. Using Eq. (9) we write the electromagnetic fields in terms of the scalar Debye potentials as follows:

$$\begin{aligned}\mathbf{E} &= \nabla \times \nabla \times (\mathbf{r} \Pi^E) + i\omega\mu \nabla \times (\mathbf{r} \Pi^M) \\ \mathbf{H} &= \nabla \times \nabla \times (\mathbf{r} \Pi^M) - i\omega\epsilon \nabla \times (\mathbf{r} \Pi^E).\end{aligned}\quad (10)$$

C. Mie-Debye theory of optical tweezers for chiral sphere

As it is depicted in Fig. 1, an optical tweezers setup consists of a laser beam strongly focused by a high numerical aperture (NA) objective. Stable trapping in the focal region is possible for certain “goldilocks” combinations of the optical properties of the object to be trapped and the surrounding medium. We consider a 1064 nm Gaussian beam, circularly polarized with helicity σ , at the objective entrance port. The beam is focused by the objective into the sample region containing an aqueous suspension (refractive index $n_w = \sqrt{\epsilon_w}$) of homogeneous chiral spheres, with effective relative permittivity ϵ_s and chirality κ . The focused beam in the sample region is represented in terms of the so called Richards-Wolf integral representation [41, 51]

$$\begin{aligned}\mathbf{E}_{\text{in}}(\mathbf{r}) &= E_0 \int_0^{2\pi} d\varphi_k \int_0^{\theta_0} d\theta_k \sin \theta_k \sqrt{\cos \theta_k} e^{-\gamma_f^2 \sin^2 \theta_k} \\ &\quad \times e^{i\mathbf{k}(\theta_k, \varphi_k) \cdot (\mathbf{r} + \mathbf{r}_s)} \hat{\mathbf{e}}'_\sigma(\theta_k, \varphi_k),\end{aligned}\quad (11)$$

where we set the origin at the center of the sphere and the focal point is at position $-\mathbf{r}_s$. The region of integration in Fourier space is defined by the angle θ_0 , which in turn depends on the objective numerical aperture NA: $\sin \theta_0 = \min\{1, \text{NA}/n_w\}$. γ_f is the ratio of the objective focal length to the laser beam waist at the objective entrance port and $\hat{\mathbf{e}}'_\sigma(\theta_k, \varphi_k) = \hat{\mathbf{x}}'(\theta_k, \varphi_k) + i\sigma \hat{\mathbf{y}}'(\theta_k, \varphi_k)$. The unit vectors $\hat{\mathbf{x}}'(\theta_k, \varphi_k)$ and $\hat{\mathbf{y}}'(\theta_k, \varphi_k)$ are obtained from $\hat{\mathbf{x}}$ and $\hat{\mathbf{y}}$ by rotation with Euler angles $\alpha = \varphi_k$, $\beta = \theta_k$ and $\gamma = -\varphi_k$. We have assumed an ideal aplanatic optical system when writing Eq. (11). Optical aberrations can be included as additional phase factors in the integrand in the r.-h.-s. of (11) [52] and the resulting optical force can be derived by following the steps presented below.

We take $\mathbf{E}_{\text{in}}(\mathbf{r})$ as the incident field on the chiral microsphere. The strategy is to take each plane wave component of Eq. (11), solve the scattering problem using the

results of section II B, and superpose the solutions appropriately. There is, however, a caveat: the expressions in last section assume a $\hat{\mathbf{z}}$ -propagating incident wave, and in (11) we have components propagating in many different directions, so we must rotate our coordinate system in order to have the solution for an arbitrary incident wave. This is accomplished by the matrix elements of finite rotations $d_{m,m'}^j(\theta)$ [53]. After these operations, the Debye potentials associated to an incident circular polarized plane wave (helicity σ) propagating along an arbitrary direction defined by the spherical angles (θ_k, ϕ_k) are given by

$$\begin{aligned}\Pi_{\mathbf{k},\sigma}^{E,\text{in}}(r, \theta, \phi) &= \sigma \frac{iE_0}{k} \sum_{\ell} i^{\ell} j_{\ell}(kr) \sqrt{\frac{4\pi(2\ell+1)}{\ell(\ell+1)}} Y_{\ell}^{(\sigma)}(\theta, \phi) \\ \Pi_{\mathbf{k},\sigma}^{M,\text{in}}(r, \theta, \phi) &= \frac{E_0}{k} \sum_{\ell} i^{\ell} j_{\ell}(kr) \sqrt{\frac{4\pi(2\ell+1)}{\ell(\ell+1)}} Y_{\ell}^{(\sigma)}(\theta, \phi),\end{aligned}\quad (12)$$

where $j_{\ell}(x)$ are the spherical Bessel functions [50] and

$$Y_{\ell}^{(\sigma)}(\theta, \phi) := \sum_{m=-\ell}^{\ell} Y_{\ell m}(\theta, \phi) e^{-i\phi_k(m-\sigma)} d_{m,\sigma}^{\ell}(\theta_k).$$

Solving the scattering problem for general θ_k and ϕ_k , superposing the solutions according to (11), and undertaking a translation to a coordinate system centered at the focal point — so that the sphere’s center is finally at position \mathbf{r}_s —, we arrive at the Debye potentials for the total fields

$$\begin{aligned}\Pi_{\sigma}^{E,\text{tot}} &= \sigma \frac{iE_0}{k} \sum_{\ell,m} i^{\ell} \gamma_{\ell,m}^{\sigma} [j_{\ell}(kr) - (a_{\ell} + i\sigma d_{\ell})h_{\ell}(kr)] \times \\ &\quad Y_{\ell m}(\theta, \phi) e^{-i(m-\sigma)\phi_s}\end{aligned}\quad (13)$$

$$\begin{aligned}\Pi_{\sigma}^{M,\text{tot}} &= \frac{E_0}{k} \sum_{\ell,m} i^{\ell} \gamma_{\ell,m}^{\sigma} [j_{\ell}(kr) - (b_{\ell} - i\sigma c_{\ell})h_{\ell}(kr)] \times \\ &\quad Y_{\ell m}(\theta, \phi) e^{-i(m-\sigma)\phi_s},\end{aligned}\quad (14)$$

where $h_{\ell}(kr)$ is the spherical Hankel function of the first kind. The coefficients

$$\begin{aligned}\gamma_{\ell,m}^{\sigma} &= 2\pi \sqrt{\frac{4\pi(2\ell+1)}{\ell(\ell+1)}} (-i)^{m-\sigma} \int_0^{\theta_0} d\theta_k \sin \theta_k \times \\ &\quad \sqrt{\cos \theta_k} d_{m,\sigma}^{\ell}(\theta_k) J_{m-\sigma}(k\rho_s \sin \theta_k) e^{ikz_s \cos \theta_k}\end{aligned}\quad (15)$$

are written in terms of the cylindrical Bessel functions $J_{m-\sigma}$ of integer order $m-\sigma$.

Here we have expressed the microsphere position $\mathbf{r}_s = (\rho_s, \varphi_s, z_s)$ in cylindrical coordinates. When taking κ to zero ($c_{\ell} = d_{\ell} = 0$) we recover the Debye potentials for an achiral sphere [41]. However, the most interesting property of Eqs. (14) is that they have the same form as the Debye potentials of an achiral sphere, provided the following replacements are made

$$A_{\ell} \leftrightarrow a_{\ell} + i\sigma d_{\ell} \quad (16)$$

$$B_{\ell} \leftrightarrow b_{\ell} - i\sigma c_{\ell}, \quad (17)$$

where A_ℓ and B_ℓ would be the Mie coefficients of the equivalent achiral sphere scattering a circularly polarized beam of helicity σ . Equations (16) and (17) show that one can map the problem of light scattering by a homogeneous chiral sphere into the simpler original Mie scattering problem.

As the final step in the derivation, we compute the optical force upon the sphere by integration of the Maxwell stress tensor:

$$\mathbf{F} = \lim_{r \rightarrow \infty} \left[-\frac{r}{2} \int_S \mathbf{r} (\epsilon_w \epsilon_0 E_{\text{tot}}^2 + \mu_0 H_{\text{tot}}^2) d\Omega \right] \quad (18)$$

where \mathbf{E}_{tot} and \mathbf{B}_{tot} are the total electric and magnetic fields and the Gaussian spherical surface S is taken at infinity. At this point it is useful to define the (dimensionless) efficiency factor \mathbf{Q}

$$\mathbf{Q} = \frac{c}{n_w P} \mathbf{F}, \quad (19)$$

where \mathbf{F} is given by (18), P is the incident laser power at the sample region and c is speed of light. The efficiency may be conveniently split into extinction and scattering terms

$$\mathbf{Q} = \mathbf{Q}_e + \mathbf{Q}_s, \quad (20)$$

where the extinction term \mathbf{Q}_e is connected to the rate of momentum removal from the incident beam. Part of this momentum ends up in the scattered field at a (normalized) rate $-\mathbf{Q}_s$, so the total (normalized) momentum transfer rate to the particle is $\mathbf{Q}_e + \mathbf{Q}_s$. After a long but straightforward calculation [40, 41], we get the expressions for the efficiency components Q_z , Q_s and Q_ϕ , related to the axial, radial and azimuthal force components, respectively. Explicitly, we have

- Extinction components

$$Q_{ez}(\rho_s, z_s) = \frac{4\gamma_f^2}{AN} \text{Re} \sum_{\ell m} (2\ell + 1) G_{\ell, m}^{(\sigma)} (A_\ell + B_\ell) G_{\ell, m}^{\prime(\sigma)*}, \quad (21)$$

$$Q_{e\rho}(\rho_s, z_s) = \frac{2\gamma_f^2}{AN} \text{Im} \sum_{\ell m} (2\ell + 1) G_{\ell, m}^{(\sigma)} (A_\ell + B_\ell) \left(G_{\ell, m+1}^{(\sigma)-} - G_{\ell, m-1}^{(\sigma)+} \right)^* \quad (22)$$

$$Q_{e\phi}(\rho_s, z_s) = -\frac{2\gamma_f^2}{AN} \text{Re} \sum_{\ell m} (2\ell + 1) G_{\ell, m}^{(\sigma)} (A_\ell + B_\ell) \left(G_{\ell, m-1}^{(\sigma)+} + G_{\ell, m+1}^{(\sigma)-} \right)^* \quad (23)$$

- Scattering components

$$Q_{sz}(\rho_s, z_s) = -\frac{8\gamma_f^2}{AN} \text{Re} \sum_{\ell m} \frac{\sqrt{\ell(\ell+2)(\ell+m+1)(\ell-m+1)}}{\ell+1} (A_\ell A_{\ell+1}^* + B_\ell B_{\ell+1}^*) G_{\ell, m}^{(\sigma)} G_{\ell+1, m}^{(\sigma)*} - \frac{8\gamma_f^2}{AN} \sigma \text{Re} \sum_{\ell m} \frac{(2\ell+1)}{\ell(\ell+1)} m A_\ell B_\ell^* |G_{\ell, m}^{(\sigma)}|^2, \quad (24)$$

$$Q_{s\rho}(\rho_s, z_s) = \frac{4\gamma_f^2}{AN} \sum_{\ell m} \frac{\sqrt{\ell(\ell+2)(\ell+m+1)(\ell+m+2)}}{\ell+1} \text{Im} \left\{ (A_\ell A_{\ell+1}^* + B_\ell B_{\ell+1}^*) \left[G_{\ell, m}^{(\sigma)} G_{\ell+1, m+1}^{(\sigma)*} + G_{\ell, -m}^{(\sigma)} G_{\ell+1, -(m+1)}^{(\sigma)*} \right] \right\} - \frac{8\gamma_f^2}{AN} \sigma \sum_{\ell m} \frac{(2\ell+1)}{\ell(\ell+1)} \sqrt{(\ell-m)(\ell+m+1)} \text{Re}(A_\ell B_\ell^*) \text{Im}(G_{\ell, m}^{(\sigma)} G_{\ell, m+1}^{(\sigma)*}) \quad (25)$$

$$Q_{s\phi}(\rho_s, z_s) = -\frac{4\gamma_f^2}{AN} \sum_{\ell m} \frac{\sqrt{\ell(\ell+2)(\ell+m+1)(\ell+m+2)}}{\ell+1} \text{Re} \left\{ (A_\ell A_{\ell+1}^* + B_\ell B_{\ell+1}^*) \left[G_{\ell, m}^{(\sigma)} G_{\ell+1, m+1}^{(\sigma)*} - G_{\ell, -m}^{(\sigma)} G_{\ell+1, -(m+1)}^{(\sigma)*} \right] \right\} + \frac{8\gamma_f^2}{AN} \sigma \sum_{\ell m} \frac{(2\ell+1)}{\ell(\ell+1)} \sqrt{(\ell-m)(\ell+m+1)} \text{Re}(A_\ell B_\ell^*) \text{Re}(G_{\ell, m}^{(\sigma)} G_{\ell, m+1}^{(\sigma)*}), \quad (26)$$

We have defined $A = 1 - e^{-2\gamma_f^2 \sin^2 \theta_0}$ as the fraction

of the trapping beam power that fills the objective en-

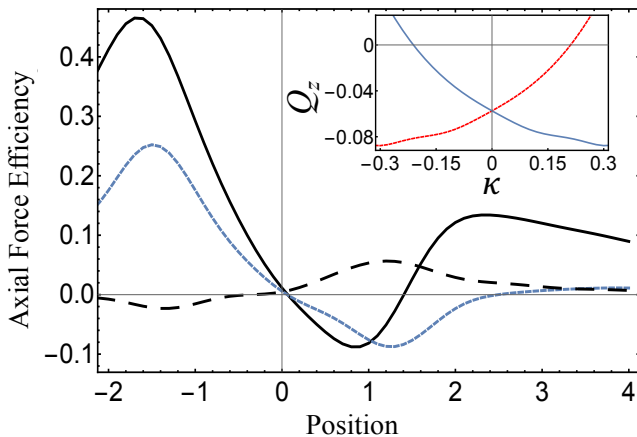


FIG. 2: Dimensionless axial force efficiency Q_z as a function of position (in units of sphere radius) along the laser axis for different values of the chirality parameter: $\kappa = -0.3$ (black line), $\kappa = 0$ (dotted line) and $\kappa = 0.3$ (dashed line). The incident beam is right-circularly polarized ($\sigma = -1$) and the microsphere radius is $a = 1 \mu\text{m}$. Inset: Q_z as a function of κ at a fixed axial position $z/a = 1.2$ for $\sigma = -1$ (red dotted line) and $\sigma = 1$ (blue line).

trance aperture and propagates into the sample. Explicit expressions for the multipole coefficients $G_{\ell m}^{(\sigma)}$, $G'_{\ell m}^{(\sigma)}$ and $G_{\ell m}^{(\sigma)\pm}$ are given in the appendix.

III. RESULTS AND DISCUSSION

In this section, we present our numerical results for the optical forces and optical torques in the framework of the MDSA formalism derived in Sec. II. In all the following examples we take the refractive indexes of the sphere and aqueous suspension to be $n_s = 1.58$ and $n_w = 1.332$, respectively. The vacuum wavelength of the laser beam is $\lambda_0 = 2\pi/k_0 = 1064 \text{ nm}$, and the other relevant parameters are $\gamma_f = 1.226$ and $\text{NA} = 1.4$.

A. Optical trapping

Due to axial symmetry, it is sufficient to analyze the optical force F_z to ensure 3-D trapping stability of optical trap. In Fig. 2, we calculate the normalized axial force acting on a microsphere as a function of sphere position along the laser axis when taking right-circular polarization (RCP), which corresponds to helicity $\sigma = -1$. We clearly see an enantioselection effect taking place. For instance, the RCP beam attracts the right-handed chiral particles with $\kappa = -0.3$ (black line) towards the paraxial focal plane with stable equilibrium position close to the focus and repels the left-handed chiral enantiomer with $\kappa = 0.3$ out of the illuminated area (dashed line). Due to mirror symmetry, this result is exactly reversed for left circularly polarized (LCP) beams, so that in this case

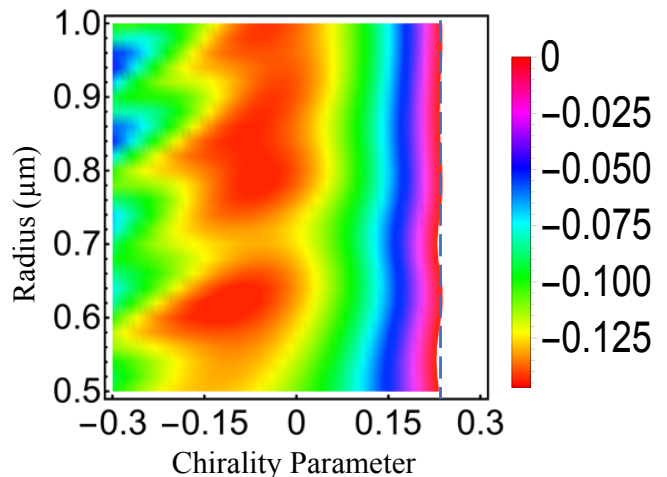


FIG. 3: Density plot of the dimensionless axial force efficiency Q_z at axial position $z/a = 1.2$. The horizontal and vertical axes represent the chirality parameter and the microsphere radius, respectively. Only negative values of Q_z are represented by the color scale. The vertical line indicates the critical value κ_0 above which no trapping takes place as the optical force becomes positive.

the spheres with positive chirality get trapped. This is illustrated by the inset of Fig. 2, where we plot the normalized axial force as a function of chirality for left and right polarization of the beam. Therefore, in a racemic mixture one could potentially use this effect to trap exclusively right- or left-handed particles by using a RCP or a LCP beam. In addition, from the inset of Fig. 2 it is also clear that despite favoring “same sign” trapping (RCP traps right-handed particles and vice versa), “opposite sign” trapping is also possible up to a critical value $|\kappa_0| \approx 0.22$.

We analyse more thoroughly the interplay of chirality and particle size in Fig. 3. The colored area shows the negative optical force (trapping force) on right handed chiral enantiomers for RCP incident light. The most important feature of this plot is the weak dependence of the force upon the sphere radius, at least for the range considered. This means that, at least for sufficiently large values of κ , the enantioselection effect is quite robust against variation of the radius, and could be effective even in solutions where the spheres size dispersion is large. It is important to emphasize that such values of κ are within the reach of state-of-the-art plasmonic and metamaterial chiral nanoparticles [14, 27, 39].

B. Optical torque

In the preceding section, we have shown that one can perform chiral resolution of a racemic mixture by selective trapping of chiral enantiomers that match the handedness of the laser beam. In this section, we discuss another method that is based on the transfer of spin angular

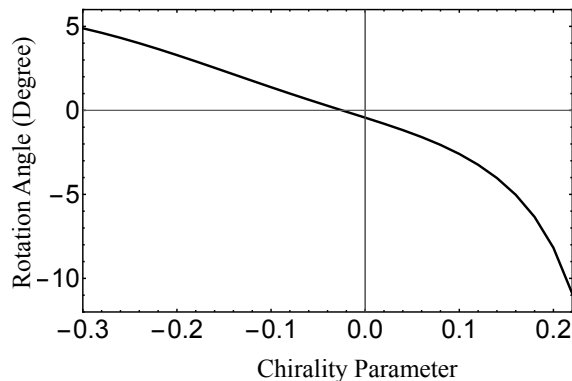


FIG. 4: Rotation angle α of a chiral microsphere of radius $a = 0.6 \mu\text{m}$ as a function of the chirality parameter κ . The incident beam is right-circularly polarized ($\sigma = -1$).

momentum (SAM) from the focused beam to the trapped microsphere, allowing to determine the chiral parameter of single particles.

In order to exploit the SAM transfer, first we stably trap a microsphere and then produce a water flow by driving the sample laterally (say, along the x -direction), as indicated in Fig. 1. A drag force F_S is then generated along the x -direction, that displaces the sphere away from the center of the optical trap and gives rise to a restoring force F_ρ . In addition, when the trapping beam is circularly polarized, it is intuitive that by pushing the sphere away from the beam axis we should also get a force along the azimuthal direction F_ϕ , as illustrated in Fig. 1. This azimuthal force component essentially converts (some of) the spin angular momentum of the beam to angular momentum of the sphere, until it equilibrates at an angle $\alpha = \arctan(F_\phi/F_\rho)$. Explicit expressions for such force components were given in Sec. II. It is more than reasonable to expect that such equilibrium angle should depend considerably upon the sphere chirality, and that is precisely what we show below.

Fig. 4 shows the optical torque exerted on the sphere in terms of the rotation angle α in degrees for a RCP trapping beam ($\sigma = -1$). First of all, it is important to mention that for a small decrease in the chirality parameter of magnitude $\delta\kappa = 10^{-2}$ the sphere undergoes a measurable additional rotation of $\delta\alpha = 0.2 - 0.5$ degrees (with the largest variation for the highest positive values of κ shown in the figure). Such strong variation of the rotation angle suggests a suitable scheme to determine and characterize the chiral parameter of a single particle, which remains a challenging task so far [11].

When the rotation angle becomes positive for negative values of κ in Fig. 4, it means that the scattered field carries a magnitude of angular momentum that exceeds that of the incident field [54], so that conservation of angular momentum leads to a torque opposite to the input spin. Such negative torque corresponds to a positive rotation angle α because we take $\sigma = -1$ here. By increasing the value of κ , the rotation angle not only changes its sign

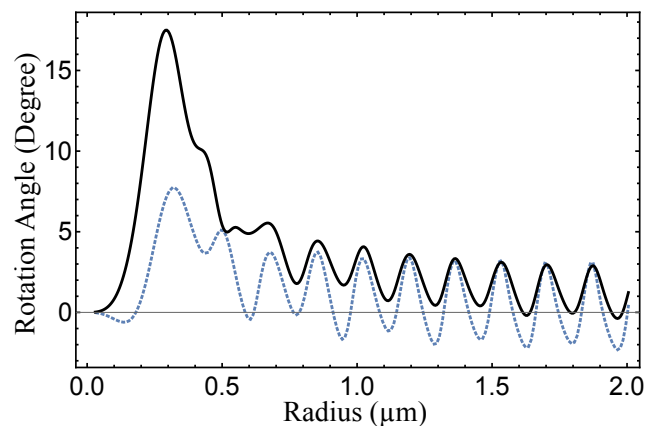


FIG. 5: Microsphere rotation angle versus sphere radius. The solid and dotted lines correspond to $\kappa = -0.3$ and $\kappa = 0$, respectively. The incident beam is right-circularly polarized ($\sigma = -1$).

but also achieves very large values in comparison to the case of achiral homogenous spheres treated so far [54], showing that chirality leads to a significant enhancement of the light-particle angular momentum transfer.

Figure 4 also shows that α changes its sign at a relative small value, $\kappa \approx -0.02$. This result demonstrates that enantioselection can also be attained by detecting the sign of the rotation angle of a particle trapped using optical tweezers, in addition to the previous chiral resolution mechanism based on selective trapping of particles of a given handedness, as previously presented.

In Fig. 5, we plot the variation of the rotation angle α versus the microsphere radius for two fixed values of the chirality parameter: $\kappa = -0.3$ (solid) and $\kappa = 0$ (dotted). As in Fig. 4, we take RCP corresponding to $\sigma = -1$. For small microspheres the rotation angle is negative for achiral particles (positive torque) and positive for $\kappa = -0.3$ (negative torque). In the Rayleigh scattering regime, $a \ll \lambda_0$, scattering is weak and both force and torque are dominated by the extinction contribution. Indeed, very small particles behave as local probes of the input angular momentum, thus explaining the negative angles in the case of small achiral spheres. On the other hand, Fig. 5 shows that the particle chirality strongly affects the sign of the optical torque even in the Rayleigh limit.

As the size parameter increases light scattering becomes more prominent and the transfer of angular momentum is amplified [55], leading to much larger angles as illustrated by Fig. 5. In particular, we find a peak value around $a \approx 0.3 \mu\text{m}$ of approximately 17° . Such a large rotation angle cannot be obtained with achiral microspheres [54]. As the radius is further increased into the ray optics range, the rotation angle for the achiral sphere oscillates around zero, which is compatible with the vanishing optical torque in the ray optics approximation [41], whereas the curve for the chiral particle

suggests a nonzero torque in this limit.

IV. CONCLUSIONS

In this paper we developed the theory of optical tweezing for optically active homogeneous microspheres. First we developed the Bohren decomposition in terms of Debye potentials representing the incident and scattered field. Then we used the Maxwell stress tensor to calculate the optical forces exerted on chiral spheres. Our numerical analysis predicts that circularly polarized light exerts different optical forces on left- and right-handed chiral microspheres, allowing for enantioselection. We also have shown that angular momentum transfer is different for chiral microspheres of opposite handedness, which not only greatly enhances optical rotation of the microsphere with respect to the achiral case treated so far but also leads to another chiral resolution method based on enantioselective optical torque. Altogether our findings pave the way for alternative chiral resolution methods based on optical tweezing and characterisation of chirality for the important class of homogeneous chiral microspheres,

each and every one with its individual, unique chiral response.

Acknowledgments

We thank D. S. Ether jr and N. B. Viana for inspiring discussions. This work has been supported by the Brazilian agencies National Council for Scientific and Technological Development (CNPq), Coordination for the Improvement of Higher Education Personnel (CAPES), the National Institute of Science and Technology Complex Fluids (INCT-FCx), and the Research Foundations of the States of Minas Gerais (FAPEMIG), Rio de Janeiro (FAPERJ) and São Paulo (FAPESP).

Appendix A: Multipole coefficients of the focused beam

The multipole coefficients in expressions (21)-(26) are given by

$$G_{\ell m}^{(\sigma)}(\rho_s, z_s) = \int_0^{\theta_0} d\theta \sin \theta \sqrt{\cos \theta} e^{-\gamma_f^2 \sin^2 \theta} d_{m, \sigma}^{\ell}(\theta) J_{m-\sigma}(k \rho_s \sin \theta) e^{i k \cos \theta z_s}, \quad (\text{A1})$$

$$G_{\ell, m}^{(\sigma)}(\rho_s, z_s) = \int_0^{\theta_0} d\theta \sin \theta (\cos \theta)^{3/2} e^{-\gamma_f^2 \sin^2 \theta} d_{m, \sigma}^{\ell}(\theta) J_{m-\sigma}(k \rho_s \sin \theta) e^{i k \cos \theta z_s}, \quad (\text{A2})$$

$$G_{\ell, m}^{(\sigma)\pm}(\rho_s, z_s) = \int_0^{\theta_0} d\theta \sin^2 \theta \sqrt{\cos \theta} e^{-\gamma_f^2 \sin^2 \theta} d_{m \pm 1, \sigma}^{\ell}(\theta) J_{m-\sigma}(k \rho_s \sin \theta) e^{i k \cos \theta z_s}, \quad (\text{A3})$$

where $k = n_w k_0$ is the wavenumber in the aqueous host medium. The corresponding wavevector makes an angle

θ with respect to the optical z -axis.

-
- [1] G. H. Wagnière, *On chirality and the universal asymmetry: reflections on image and mirror image*, Wiley-VCH, Zurich, (2007).
 - [2] J. B. Pendry, *A chiral route to negative refraction*, Science **306**, 1353 (2004).
 - [3] E. Plum, J. Zhou, J. Dong, V. A. Fedotov, T. Koschny, C. M. Soukoulis, and N. I. Zheludev, *Metamaterial with negative index due to chirality*, Phys. Rev. B **79**, 035407 (2009).
 - [4] J. K. Gansel, M. Thiel, M. S. Rill, M. Decker, K. Bade, V. Saile, G. von Freymann, S. Linden, and M. Wegener, *Gold helix photonic metamaterial as broadband circular polarizer*, Science **325**, 1513 (2009).
 - [5] Y. Tang and A. Cohen, *Enhanced enantioselectivity in excitation of chiral molecules by superchiral light*, Science **332**, 333 (2011).
 - [6] M. J. Urban, C. Shen, X.-T. Kong, C. Zhu, A. O. Govorov, Q. Wang, M. Hentschel, N. Liu, *Chiral plasmonic nanostructures enabled by bottom-up approaches*, Ann. Rev. of Phy. Chem. **70**, 275 (2019).
 - [7] M. Hentschel, M. Schaferling, X. Duan, H. Giessen, and N. Liu, *Chiral plasmonics*, Science Advances **3**, e1602735 (2017).
 - [8] X.-T. Kong, L. V. Besteiro, Z. Wang, and A. O. Govorov, *Plasmonic chirality and circular dichroism in bioassembled and nonbiological systems: theoretical background*

- and recent progress Adv. Mater. 1801790 (2018).
- [9] Z. Fan, A. O. Govorov, *Plasmonic circular dichroism of chiral metal nanoparticle assemblies*, Nano Lett. **10**, 2580 (2010).
 - [10] F. A. Pinheiro, V. A. Fedotov, N. Papasimakis, and N. I. Zheludev, *Spontaneous natural optical activity in disordered media*, Phys. Rev. B **95**, 220201(R) (2017).
 - [11] Y. Zhao and J. Dionne, *Response to "Comment on enantioselective optical trapping of chiral nanoparticles with plasmonic tweezers"*, ACS Photonics **5**, 2535 (2018).
 - [12] A. J. Mastroianni, S. A. Claridge, P. Alivisatos, *Pyramidal and chiral groupings of gold nanocrystals assembled using DNA scaffolds*, J. Am. Chem. Soc. **131**, 8455 (2009).
 - [13] R. Ali, F. A. Pinheiro, R.S. Dutra, F. S. S. Rosa, and P. A. Maia Neto, *Enantioselective manipulation of single chiral nanoparticles using optical tweezers*, Nanoscale, **12**, 5031 (2020).
 - [14] S. B. Wang and C.T. Chan, *Lateral optical force on chiral particles near a surface*, Nat. Commun. **5**, 3307 (2014).
 - [15] A. Hayat, J. B. Mueller, and F. Capasso, *Lateral chirality-sorting optical forces*, Proc. Natl. Acad. Sci. U.S.A. **112**, 13190 (2015).
 - [16] A. Canaguier-Durand and C. Genet, *Plasmonic lateral forces on chiral spheres*, J. Opt. **18**, 015007 (2016).
 - [17] H. Chen, C. Liang, S. Liu, and Z. Lin, *Chirality sorting using two-wave-interference-induced lateral optical force*, Phys. Rev. A **93**, 053833 (2016).
 - [18] T. Zhang, M. R. C. Mahdy, Y. Liu, J. H. Teng, C. T. Lim, Z. Wang, and C.-W. Qiu, *All-optical chirality-sensitive sorting via reversible lateral forces in interference fields*, ACS Nano **11**, 4292 (2017).
 - [19] T. Cao and Y. Qiu, *Lateral sorting of chiral nanoparticles using Fano-enhanced chiral force in visible region*, Nanoscale **10**, 566 (2018).
 - [20] M. H. Alizadeh and B. M. Reinhard, *Enhanced optical chirality through locally excited surface plasmon polaritons*, ACS Photonics **2**, 1780 (2015).
 - [21] Y. Li, C. Bruder, and C. Sun, *Generalized Stern-Gerlach effect for chiral molecules*, Phys. Rev. Lett. **99**, 130403 (2007).
 - [22] B. Spivak and A. Andreev, *Photoinduced separation of chiral isomers in a classical buffer gas*, Phys. Rev. Lett. **102**, 063004 (2009).
 - [23] X. Li and M. Shapiro, *Theory of the optical spatial separation of racemic mixtures of chiral molecules*, J. Chem. Phys. **132**, 194315 (2010).
 - [24] R. P. Cameron, S. M. Barnett, and A. M. Yao, *Discriminatory optical force for chiral molecules*, New J. Phys. **16**, 013020 (2014).
 - [25] A. Canaguier-Durand, J. A. Hutchison, C. Genet, and T. W. Ebbesen, *Mechanical separation of chiral dipoles by chiral light*, New J. Phys. **15**, 123037 (2013).
 - [26] D. S. Bradshaw and D. L. Andrews, *Chiral discrimination in optical trapping and manipulation*, New J. Phys. **16**, 103021 (2014).
 - [27] Y. Zhao, A. A. Saleh, and J. A. Dionne, *Enantioselective optical trapping of chiral nanoparticles with plasmonic tweezers*, ACS Photonics **3**, 304 (2016).
 - [28] P. Acebal, L. Carretero, and S. Blaya, *Design of an optical conveyor for selective separation of a mixture of enantiomers*, Opt. Express **25**, 32290 (2017).
 - [29] C.-S. Ho, A. Garcia-Etxarri, Y. Zhao, and J. Dionne, *Enhancing enantioselective absorption using dielectric nanospheres*, ACS Photonics, **4**, 197 (2017).
 - [30] M. L. Solomon, J. Hu, M. Lawrence, A. Garcia-Etxarri, J. A. Dionne, *Enantiospecific optical enhancement of chiral sensing and separation with dielectric metasurfaces*, ACS Photonics **6**, 43 (2018).
 - [31] R. J. Hernandez, A. Mazzulla, A. Pane, K. Volke-Sepulveda, and G. Cipparrone, *Attractive-repulsive dynamics on light-responsive chiral microparticles induced by polarized tweezers*, Lab Chip **13**, 459 (2013).
 - [32] G. Tkachenko and E. Brasselet, *Optofluidic sorting of material chirality by chiral light*, Nat. Commun. **5**, 3577 (2014).
 - [33] M. Donato, J. Hernandez, A. Mazzulla, C. Provenzano, R. Saija, R. Sayed, S. Vasi, A. Magazzu, P. Pagliusi, R. Bartolino, P. Gucciardi, O. Marago, and G. Cipparrone, *Polarization-dependent optomechanics mediated by chiral microresonators*, Nat. Commun. **5**, 3656 (2014).
 - [34] G. Tkachenko and E. Brasselet, *Helicity-dependent three-dimensional optical trapping of chiral microparticles*, Nat. Commun. **5**, 4491 (2014).
 - [35] Y. Zhao *et al.*, *Nanoscope control and quantification of enantioselective optical forces*, Nat. nanotechnology **12**, 1055 (2017).
 - [36] G. Schnoering, L. V. Poulikakos, Y. Rosales-Cabara, A. Canaguier-Durand, D. J. Norris, and C. Genet, *Three-dimensional enantiomeric recognition of optically trapped single chiral nanoparticles*, Phys. Rev. Lett. **121**, 023902 (2018).
 - [37] N. Kravets, A. Aleksanyan, and E. Brasselet, *Chiral optical Stern-Gerlach Newtonian experiment*, Phys. Rev. Lett. **122**, 024301 (2019).
 - [38] N. Kravets, A. Aleksanyan, H. Chraibi, J. Leng, and E. Brasselet, *Optical enantioseparation of racemic emulsions of chiral microparticles*, Phys. Rev. App. **11**, 044025 (2019).
 - [39] Z. Fan, A. O. Govorov, *Chiral nanocrystals: plasmonic spectra and circular dichroism*, Nano Lett. **12**, 3283 (2012).
 - [40] P. A. Maia Neto and H. M. Nussenzveig, *Theory of optical tweezers*, Europhys. Lett. **50**, 702 (2000).
 - [41] A. Mazolli, P. A. Maia Neto, H. M. Nussenzveig, *Theory of trapping forces in optical tweezers*, Proc. R. Soc. Lond. A, **459**, 3041 (2003).
 - [42] V. Lindell, A. H. Sihvola, S. A. Tretyakov, and A. J. Vititanen, *Electromagnetic waves in chiral and bi-isotropic media*, (Artech House, Boston, 1994).
 - [43] A. Lakhtakia and V. V. Varadan, *Time-harmonic electromagnetic fields in chiral media*, (Springer-Verlag, Berlin, 1989).
 - [44] H. Chen, N. Wang, Wanli L., Shiyang Liu, and Zhifang Lin, *Tailoring azimuthal optical force on lossy chiral particles in Bessel beams*, Phys. Rev. A, **90**, 043850 (2014).
 - [45] *If $\epsilon\mu = \kappa^2$ we have the chiral analogue of bulk plasmons, which are longitudinal solutions for the fields.*
 - [46] C. F. Bohren and D. R. Huffman, *Absorption and scattering of light by small particles* (Wiley, New York, 1998).
 - [47] M. Born and E. Wolf, *Principles of Optics*, (Pergamon, Oxford, 1980).
 - [48] C.R. Bohren, *Light scattering by an optically active sphere*, Chem. Phys. Lett. **29**, 458 (1974).
 - [49] Q. Shang, Z. Wu, Tan Qu, Z. Li, Lu Bai, and L. Gong, *Analysis of the radiation force and torque exerted on a chiral sphere by a Gaussian beam*, Opt. Exp. **21**, 8677 (2013).

- [50] M. Abramowitz and I. Stegun, *Handbook of mathematical functions*, (Dover, New York, 1972).
- [51] B. Richards and E. Wolf, *Electromagnetic diffraction in optical systems II. Structure of the image field in an aplanatic system*, Proc. R. Soc. London A **253**, 358 (1959).
- [52] R. S. Dutra, N. B. Viana, P. A. Maia Neto and H. M. Nussenzveig, *Absolute calibration of forces in optical tweezers*, Phys. Rev. A **90**, 013825 (2014).
- [53] A. R. Edmonds, *Angular momentum in quantum mechanics* (Princeton University Press, 1957).
- [54] K. Diniz, R. S. Dutra, L. B. Pires, N. B. Viana, H. M. Nussenzveig, and P. A. Maia Neto, *Negative optical torque on a microsphere in optical tweezers*, Opt. Express **27**, 5905 (2019).
- [55] D. S. Bradshaw and D. L. Andrews, *Manipulating particles with light: radiation and gradient forces*, Eur. J. Phys. **38**, 034008 (2017).